Defect detection of wire rope for oil well based on adaptive angle

Zhang Jijun, Meng Xiangqing
Southwest Petroleum University, China
790100588@qq.com, 842676523@qq.com

ABSTRACT. This paper uses a digital image processing method which is based on texture feature of steel cable to detect the fracture of steel wire. At first, it uses a modified homomorphic filtering method to eliminate environment heterogeneous shining. Next, it obtains the body image of the steel line by using the method of edge detecting and section counting filtering to detect the bunch part of steel wire. By using an improved Radon transformation method to indicate if those steel wire are in good condition or not. Finally, by using BP neural network model it aims to judge the final result. Test result shows that this method is easy to use and fulfill real time request.

KEYWORDS. Homomorphic filtering method; Edge detection; Integral projection; BP neural network.

INTRODUCTION

As a flexible component, wire rope has been widely used in engineering. The common cableway, crane, hoister and elevator have all used wire rope, it occupies an important position in industrial sectors such as metallurgy, machinery, chemical industry, oil, transportation, tourism and construction industry, etc., therefore, it directly affects people's daily life, even the development of the national economy [1].

Wire rope is high in strength, good in tenacity, as well as strong in bearing capacity, which makes low noise and exert stability during work. However, as a bearing component in engineering, it will deform, be corroded, fracture or even suddenly break down due to the load and tensile force it bears for a long time. It affects the normal operation of the equipment, even threaten the life security of the public, Great importance should be attached to its user's safety.

In the drilling platform of oil and gas in this paper, wire rope is supervised through naked-eye identification and regular replacement in order to extend the service life of wire rope and guarantee the safety of its application. However, erroneous judgment and negligence are inevitable in the check by naked eyes, and the regular replacement will also result in wasting, consuming unnecessary man power and material resource. Hence, from the view of both economic benefit and social benefit, developing a new method to defect detection of wire rope is an inexorable trend [2-3].

In order to increase the degree of intelligentization of the nondestructive testing of wire rope, improve the objective & unscientific parts and low efficiency and provide more detailed and perfect information of fracture of wire, and evaluate the damage, this paper discusses a way of defect detection of wire rope for oil well based on adaptive angle by regarding the projection features of the images of wire rope as the basis of defect identification.

DETECTION METHOD OF BROKEN WIRE ROPE

Image preprocessing based on the improved homomorphic filtering optimization algorithm

As shown in Fig. 1, the collected images all have relatively strong side light and serious degradation with uneven brightness since the experimental environment is very complex, bringing great difficulty to the following texture extraction. Thus, the images should be dealt with filtering processing to different degrees.

Figure 1: Original drawing of wire rope

Analysis shows that the background information of the image corresponds to the high-frequency part of the image, while the information of the object itself corresponds to the low-frequency part. For the image with uneven brightness, we need to weaken the low frequency component and strengthen high frequency component to reflect features of the object to the greatest extent and strengthen contrast ratio, and then conduct homomorphic filtering [4]. The classical homomorphic filtering algorithm is conducted in the frequency domain. Firstly, FFT exchanges will be made to the image, and different filter functions will be adopted for filtering according to the needs of image's the low-frequency part and high-frequency part. IFFT exchange will be conducted in the last period, and then turn the image back. There are several obvious disadvantages concerning the frequency domain algorithm. The first one is the failure to achieve the effect of local contrast enhancement; the second is that two times of FFT will reduce the efficiency of operation due to the big calculation amount of FFT. To solve these problems, Conducting homomorphic filtering on spatial domain is taken into consideration. Generally, it will firstly divide the original image into low-frequency part (incidence component) and high-frequency part (reflection component). Next, conduct filtering to the images with Gaussian Lowpass Filters to get the component of incident light. The original image subtracts the incident light to result in the reflection component. Since the incident component and reflection component are separated by taking logarithm, the true image with enhancement can be obtained with antilog operation. In addition, the thought of template factoring has improved the Gaussian Lowpass Filters and greatly reduced the space for operation and quickened the arithmetic speed, causing a satisfactory effect of homomorphic filtering. Consequently, the paper adopts spatial homomorphic filtering algorithm [5-6], to correct the brightness of the image of wire rope, so as to eliminate the influence of the uneven illumination. The detailed steps are as follows:

$f(x, y)$, function of gray level of the image can be seen as the product of the incident light and reflected light, namely:

$$f(x, y) = i(x, y) \cdot r(x, y)$$

$i(x, y)$ is incident light, and $0 < i(x, y) < \infty$, while $r(x, y)$ is the reflected light, and $0 < i(x, y) < \infty$. Then take the logarithm of the image, that is assuming:

$$z(x, y) = \ln f(x, y) = \ln i(x, y) + \ln r(x, y)$$

In this way the incident light and reflected light can be separated. In that the low-frequency part of the image is the incident light and the high-frequency part is reflected light, the left will be the low-frequency part (incident light) when we conduct Lowpass filtering to $z(x, y)$, as shown below:

$$z^{'}(x, y) = LPF\{z(x, y)\} \approx \ln i(x, y)$$

Thus, we can use the original image to subtract the image after lowpass filtering to get the image with increasing high-frequency part (reflected light):

$$s(x, y) = z(x, y) - z^{'}(x, y) \approx \ln r(x, y)$$

Finally, we should conduct antilog operation to $s(x, y)$ to achieve correct results:

$$s^{'}(x, y) = \exp[s(x, y)] \approx r(x, y)$$

However, it's clear that if we just use the original image to subtract the image after lowpass filtering, it's similar to conducting common lowpass filtering to the image, and we can get what we want. As a result, we consider conducting weighted approach on the lowpass filtering to get the expected effect of increasing high-frequency part and suppressing low-frequency part:

$$s(x, y) = z(x, y) - t z^{'}(x, y) \approx \ln r(x, y) + (1-t) \ln i(x, y)$$

Assume $u = 1 - t$, and the formula above will be:

$$s(x, y) \approx \ln r(x, y) + u \ln i(x, y)$$

u is the weighting variable, and $0 \le u \le 1$, of which the meaning is the reserved weigh of low-frequency information in the image. Next, to study the influence of value of u on the image, we will take 0.2 as step size, and conduct spatial homomorphic filtering to the original image. The results are as shown in Fig. 2.
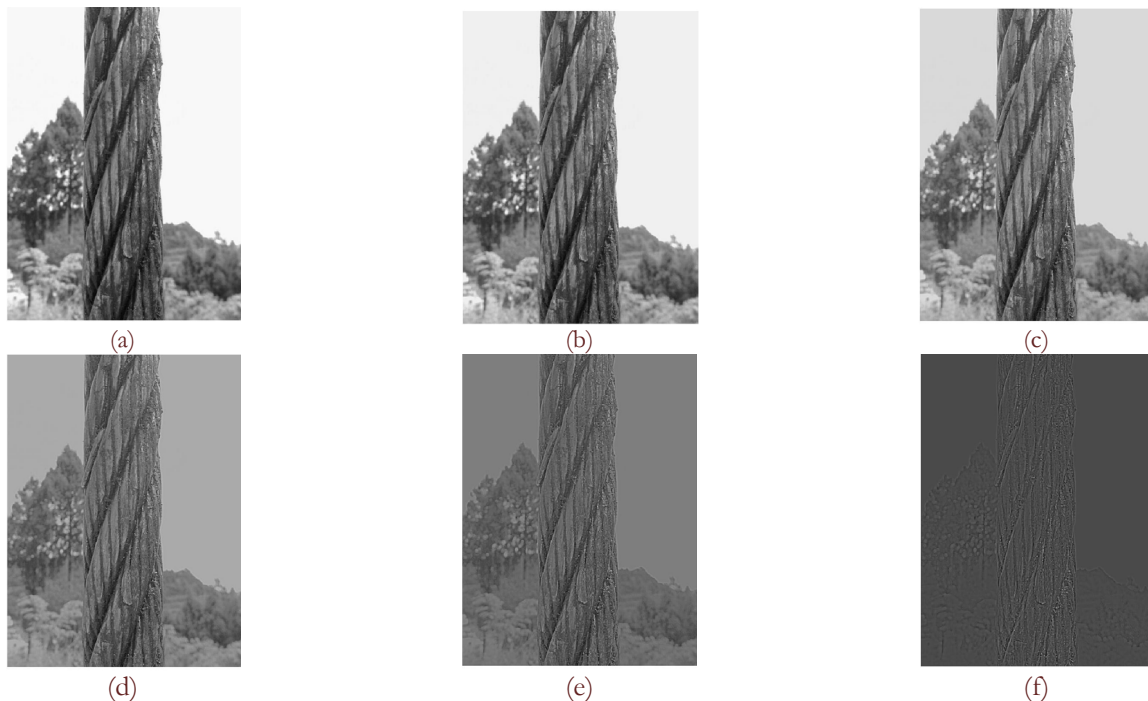

(a) (b) (c)

(d) (e) (f)

Figure 2: Figs. a-f show the effects of homomorphic filtering under 0, 0.2, 0.4, 0.6, 0.8 and 1, respectively.

From the analysis about a-f, we can infer that higher value of u indicates closer distance between the image and high-pass filtering, stressing the reflection of details, and resulting in loss of some necessary high-frequency information. Lower

value of $f(i,j)$ means the uneven brightness of the image, and bigger the interference of the background information. Therefore, we need to weigh in accordance with needs, and take weighting variables that are most suitable for effect of filtering. In this article, we take u as 0.6, and thus can get the ideal effect.

Fig. 3 tells us that the uneven brightness and shadowing are eliminated after spatial homomorphic filtering and the marginal information is strengthened.

Extraction of Wire rope

Edge is the basic feature of the image. Generally speaking, at the location of edge, the gray level will be different from that of the adjacent area, consequently it will draw the outline of the target object [7-9]. This article uses Roberts operator to detect edge [10-11], and get the edge image. Roberts uses the performance of the partial difference operator to find out the operator of the edge. It sets $f(i,j)$ as the input image and $g(i,j)$ as output image. Roberts edge gradient is calculated by the formula below.

$$g(i,j) = \left\{ \left[f(i+1,j+1) - f(i,j) \right]^2 + \left[f(i,j+1) - f(i+1,j) \right]^2 \right\}$$

Figure 3: Effect of holomorphic filtering.

Figure 4: Roberts's operator to calculate edge.

It can be seen from the experiment that a certain quantity of noisy points have appeared during the edge detection of the image with Roberts operator, as shown in Fig. 4, which surely affecting the extraction of wire rope, conducting filtering is a necessity. It can be observed that the noise points are relatively separate and the quantity is small, resulting in a distinctive comparison with the wire rope itself at the vertical direction. This paper lists the statistical filtering to make statistics of the quantity of efficient points of each line of the image, and sets threshold value. Then the wire rope itself and the blending points of the background will be differentiated based on the results of statistics and conduct filtering, as shown in Fig. 5. In this way the extraction of the image of wire rope can be achieved, as shown in Fig. 6.
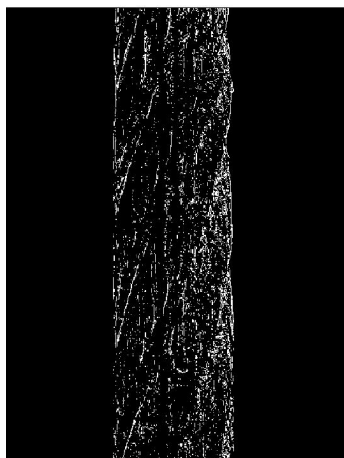

Figure 5: Denoised edge image.

Figure 6: A Sketch after background subtraction.

Extracting of the wire rope strand based on canny

To judge whether there is any defect in the wire rope after separating it from its background, we need to extract the slant texture of the wire rope strand. If the wire rope is undamaged, the texture will be complete and regular, based on which, we firstly adopt the homomorphic filtering technique to filter the image by a high pass filter to strengthen the edge information of the wire rope strand as in Fig. 7.

The gray level change based on the reflected light image can strengthen the contrast of image. The process of grey level transformation is as below:

$$g(x, y) = T[f(x, y)]$$

It turns the gray level, $f(x, y)$, of each pixel, (x, y), in the input image into the gray level, $g(x, y)$, in the output image. This article uses imadjust to transform the gray level, and the results are shown in Fig. 8.

Figure 7: Sketch after high-pass filtering.

Figure 8: Sketch after gray level transformation.

After we get the function of contrast enhancement, we need to position the edge point accurately on the pixel point that transformed to a higher grey level to restrain false edge to the best extent and reduce peripheral point. So we use Canny operator[12] to conduct the extraction of wire rope strand. The procedure is as below:

(1) Smooth the image with Gaussian filter.
(2) Calculate the gradient magnitude and direction with first-order partial finite difference.
(3) Restrain the gradient magnitude to the biggest extent.
(4) Detect and connect edges with dual threshold algorithm.

The effect is shown as Fig. 9.

Angle adaptive integral transformation

The projection feature of image obtained by integral projection [13-15] has translation invariance and can well express the distribution pattern of pixels in the space. F_{ij} is the gray level of the image at (i,j). The formulas to solve the horizontal integral projection, PY_i, of image in $[x_1, x_m]$ and the vertical integral projection, PY_j, of the image in $[x_1, x_m]$, are as below:

$$PY_i = \frac{1}{m} \sum_{i=X_1}^{X_m} F_{ij}, j = Y_1, Y_2, ..., Y_n$$

$$PY_j = \frac{1}{n} \sum_{i=Y_1}^{Y_n} F_{ij}, j = X_1, X_2, ..., X_m$$

After the edge of wire rope strand is extracted, the angle of the trend of strand cannot be accurately calculated, and because of which the Project direction and the trend direction of the strand may not match if the line integral is conducted in a fixed angle. The corresponding result may also have errors in it. Therefore, in this article, an improved horizontalprojection is adopted (by rotating the image with a fixed angular difference) to get all the projection integrals in one angle-domain. Based on the judgment of all the results generated, the best integral angle can be chosen for the most suitable image with integral projection.
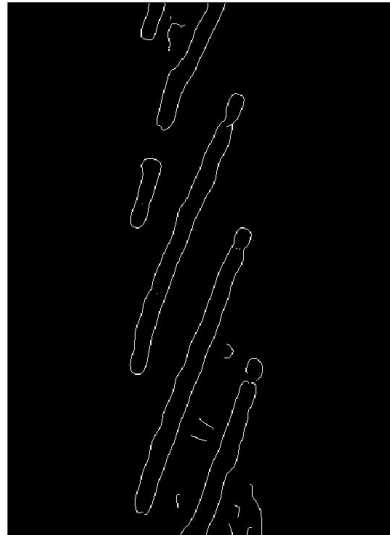

Figure 9: Sketch of the extracted edge of the wire rope strand by canny operator.

The thought to select the conditions for judgment is as below. When the integral position coincides with the edge of a wire rope strand, there will be a peak in the horizontal integral projection image, that is, the extreme point; and the strands under detection of each image under the same conditions are the same. From these angles, we can restrain the horizontal integral projection image as below. (1) Restrain the scope of the quantity of the effective extreme points, p_i, which should be two times of the quantity of strands of each picture, P, including the strands under detection, because each strand will have two extreme points. And, we can regard the $2P$ extreme points with the highest pulse are effective extreme points; (2) Restrain the height of the extreme points in the image, $f(p_i)$. When the sum of the heights of all the extreme points reaches to the peak, the direction of the integral is regarded as the same as the direction of strand.

So, when the following conditions are met, the image with the best integral angle can be obtained.

$$\begin{cases} \sum_{i=1}^{n} i \geq 2P \\ \sum_{i=1}^{n} f(p_i) = Max[\sum_{i=1}^{n} f_s(p_i)] \end{cases}$$

In the formula, $i = 1, 2, \cdots n$, which is the quantity of the extreme points of the current image, and $s = 1, 2, \cdots m$, which is the time of rotation in the angle domain.

Before conducting the angle adaptive integral transformation, a simple dilation operation shall be conducted to the image, because generally the strands of the wire rope are not absolute straight line, which may affect the effect of integral and lead to errors. So the combination of dilation operation and bold edge will achieve better effect.

After the dilation operation on Fig. 8 through steps above, the following angle adaptive integral projection will get the results as shown in Fig. 10 and 11. It's clear that we can identify where the fracture happens. In this way, not only can we judge whether the wire rope has superficial defect, but can also position the defect. The detection results meet the requirements.
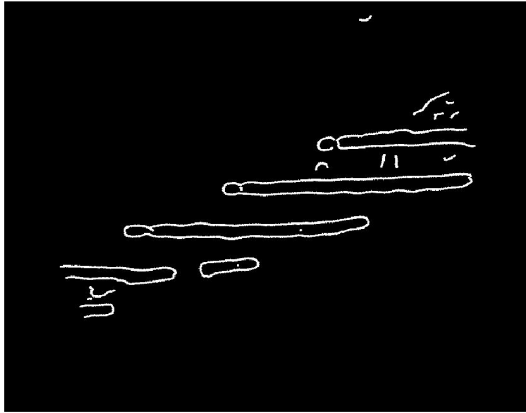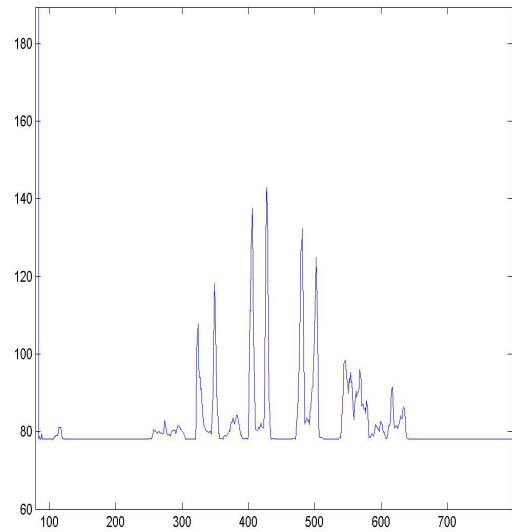
Figure 10: Results of angle adaptive method.

Figure 11: Horizontal integral projection.

Identify the defect of wire rope with neural network

Identify the superficial defect of the wire rope with BP neural network, Sigmoid function as excitation function, and error signal back propagation algorithm [16-20] as training algorithm, parameters are as below: number of nodes at input layer is 4, and the input values are respectively quantity of effective pulse, width of pulse, sum of height of pulse and radius of wire rope under detection. We can identify whether the different kinds of wire ropes have defect. Besides, the number of nodes at implicit strata is 6 and at output layer is 1. Assume the transmission function and output of the j nerve cell at L-1 layer of the k training sample are respectively $u_j^{L-1}(k)$ and $z_j^{L-1}(k)$, then:

$$\frac{\partial E}{\partial \omega_L^{ij}} = -2\sum_{k=1}^{K}\frac{\partial E}{\partial u_i^L(k)} \cdot \frac{\partial u_i^L(k)}{\partial \omega_{ij}^L}$$

$$= -2\sum_{k=1}^{K}\left[\delta_i^L(k) \cdot \frac{\partial}{\partial \omega_{ij}^L}\sum_m \omega_{im}^L z_m^{L-1}(k)\right]$$

$$= -2\sum_{k=1}^{K}\delta_i^L(k)z_j^{L-1}(k)$$

In the formula, E is the overall error; ω_L^{ij} is weight; $\delta_i(k)$ is delta error.

$$\delta_i^L(k) = \frac{\partial E}{\partial u_i^L} = \sum_{m=1}^{M}\frac{\partial E}{\partial u_m^{L+1}(k)} \cdot \frac{\partial u_m^{L+1}(k)}{\partial u_i^L(k)}$$

$$= \sum_{k=1}^{K}\left[\delta_m^{L+1}(k) \cdot \frac{\partial}{\partial u_i^L(k)}\sum_{j=1}^{J}\omega_{mj}^L f(u_j^L(k))\right]$$

$$= f'(u_j^L(k)) \cdot \sum_{m=1}^{M}\delta_m^{L+1}(k) \cdot \omega_{mi}^L$$

The renewal process of weight is as below:

$$\omega_{ij}^L(t+1) = \omega_{ij}^L(t) + \eta \cdot \sum_{k=1}^{K}\delta_i^L(k)z_j^{L-1}(k)$$

$$+ \mu\left[\omega_{ij}^L(t) - \omega_{ij}^L(t-1)\right] + \varepsilon_{ij}^L(t)$$

The last three items in the formula above are respectively gradient, temporal item and stochastic noise of the average error. In this paper, 30 images of normal wire rope and 30 images of wire rope with fractures are used for the training of the neural network model, taking learning rate, η, as 0.1, and instant constant, μ, as 0.85. The output of the wire rope with defect is 1, or otherwise, 0. At the beginning, weight is selected as the random number to meet normal distribution. Through the output results of the training set by statistics, the scope of the output threshold value can be identified. Fig. 12 shows the structure of the three layers of BP neural network, and Tab. 1 presents the results from the tests of the experimental groups.
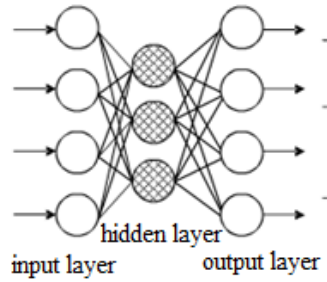

Figure 12: Structure of the three layers of BP neural network.

No.	State of wire rope	Output of neural network
1	Surface damage	0.423
2	good	0.933
3	good	0.862
4	Surface damage	0.699
5	good	0.914
6	good	0.872
7	Surface damage	0.795

Table 1: Results from the tests of the experimental groups.

Based on the actual state of the wire rope, and the corresponding output results of the neural network, this paper sets the output threshold value for identifying of the neural network model at 0.85.

RESULTS AND ANALYSIS

To verify the effectiveness of the neural network model, the collected 60 original pictures of wire rope are input as test samples into the neural network model to identify the existence of fracture. There are 30 pictures of good wire rope and 30 with defect. Through the experimental analysis, the experimental results of wire rope test are shown in Tab. 2.

State of wire rope	Good wire rope	Wire rope with defect	Accuracy
Good surface	27	3	91%
Surface damage	2	28	93.3%

Table 2: Detection results of wire rope.

It can be seen from the results that the method proposed in this paper can reach a relatively high accuracy of the defect detection of surface of wire rope, yet some errors are inevitable. Through the analysis, it indicates that the good wire rope

will are often affected by oil contamination and other dirt on the surface, which will be mistakenly identified as defect; some of the damages on the surface of wire rope are not so obvious, therefore the wire will be identified as being in good condition. But the misjudgment rate is overall low, and the misjudgment rate of the wire rope with defect on the surface is lower than that of the wires with good surface. So this can replace the manpower to detect the wire ropes.

CONCLUSION

The method of filtering realizes the separation of the texture and background of the wire ropes. The defect detection of wire rope for oil well based on angle adaptive can reach a relatively high accuracy and speed. It's applicable for the online real-time detection of the wire rope. Identifying the surface damage of wire ropes by the detection method proposed in this article can meet the needs of the actual detection.

REFERENCES

[1] Xv, J., The intelligent detection technique study for broken wires of the steel wire rope, Wuhan University of Technology, 2002.

[2] Shen, Y., Zhang, D., Ge, S., Effect of fretting amplitudes on fretting wear behavior of steel wires in coal mines, Mining Science and Technology, 20 (2010) 803-808.

[3] Zhang, D., Ge, S., Xiong, D., Fretting wear of steel wires in hoisting ropes , International Journal of Minerals Metallurgy and Materials, 9(2) (2002) 81-84.

[4] Wang, Y., Long, X., Reduce non-uniform illumination with wavelet, Optical Technique, 5 (2005) 726-728. DOI: 10.13741/j.cnki.11-1879/o4.2005.05.026

[5] Wen, S., You, Z., Performance optimization homomorphic filtering algorithm, Application Research of Computers, 3 (2000) 62-65.

[6] Bertalmío, M., Caselles, V., Provenzi, E., Issues about retinex theory and contrast enhancement, International Journal of Computer Vision, 83(1) (2009) 101-119. DOI: 10.1007/s11263-009-0221-5

[7] Ma, Y., Gu, X., Wang, Y., Feature fusion method for edge detection of color images, Journal of Systems Engineering and Electronics, 20(2) (2009) 394-399.

[8] Li, J., Huang, P., Wang, X., Pan, X., Image edge detection based on beamlet transform, Journal of Systems Engineering and Electronics, 20(1) (2009) 1-5.

[9] Dou, Z., Shi, P., Lin, Y., A kind of edge detection algorithm with edge-preserving characteristics, Journal of Harbin Institute of Technology, 20(2) (2013) 86-89.

[10] Wang, B., Using roberts operator for edge processing, Gansu Science and Technology, 10 (2008) 18-20.

[11] Ma, Y., Zhang, Z., Comparison of several edge detection operator, Industry and Mine Automation, 1 (2004) 54-56.

[12] Ding, L., Goshtasby, A., On the canny edge detector, Pattern Recognition, 34(3) (2001) 721-725. DOI: 10.1016/S0031-3203(00)00023-6.

[13] Feng, J., Liu, W., Yu, S., Eyes location based on gray-level integration projection, Computer Simulation, 4 (2005) 75-76,104.

[14] Jan, F., Usman, I., Agha, S., Reliable iris localization using integral projection function and 2D-shape properties, Chinese Optics Letters, 11 (2012) 111501(1)-111501(6). DOI: 10.3788/COL201210.111501

[15] Kim, J., Park, R., A fast feature-based block matching algorithm using integral projections, IEEE Journal on Selected Areas in Communications, 10(5) (1992) 968-971. DOI: 10.1109/49.139002

[16] Mao, L., Kong, F., et al., The wire rope surface defect detection based on image processing and neural network, Measurement & Control Technology, 7 (2007) 23-25

[17] Gao, H., Yang, S., Yang, K., et al., A neural network-based technique for quantitative wire rope inspection, NDT & E International, 26(1) (1993) 31-33.

[18] Fan, J., Du, Y., Zhou, Y., Wang, Y., Edge detection of range images using genetic neural networks, Journal of Chongqing University of Posts and Telecommunications (Natural Science Edition), 21(2) (2009) 272-275.

[19] Liu, X., Deng, Z., Wang, T., Real estate appraisal system based on GIS and BP neural network, Transactions of Nonferrous Metals Society of China, 21 (2011) 626-630. DOI: 10.1016/S1003-6326(12)61652-5.

[20] Zhang, L., Zhao, J., Zhang, X., Zhang, E., Study of a new improved PSO-BP neural network algorithm, Journal of Harbin Institute of Technology, 20(5) (2013) 106-112.